RSC Advances

PAPER

View Article Online
View Journal | View Issue

Cite this: *RSC Adv.*, 2024, **14**, 10897

Facile preparation of a CoNiS/CF electrode by SILAR for a high sensitivity non-enzymatic glucose sensor

Shi Wang, † Ruirui Zhang,† Saiwen Ding, Jialin Ao and Ting Shu *

The nanomaterials for non-enzymatic electrochemical sensors are usually pre-synthesized and coated onto electrodes by *ex situ* methods. In this work, amorphous cobalt-nickel sulfide (CoNiS) nanoparticles were facilely prepared on copper foam (CF) by the *in situ* successive ionic layer adsorption and reaction (SILAR) method, and as-prepared CoNiS/CF was studied as an electrode for non-enzymatic glucose sensing. It was analyzed by field emission scanning electron microscopy (FESEM), energy dispersive X-ray analysis (EDAX) and X-ray photoelectron spectroscopy (XPS). The electrochemical performance was investigated by cyclic voltammetry (CV) and chronoamperometry (CA). This binary sulfide electrode showed better performance toward glucose oxidation compared to the corresponding single sulfide and showed a wide linear range of 0.005 to 3.47 mM, a high sensitivity of 2298.7 μA mM^{-1} cm^{-2} and a low detection limit of 2.0 μM. The sensor exhibited high sensitivity and good repeatability and stability and was able to detect glucose in an actual sample. This work provides a simple and fast *in situ* electrode preparation method for a high-sensitivity glucose sensor.

Received 29th November 2023
Accepted 20th March 2024

DOI: 10.1039/d3ra08154k

rsc.li/rsc-advances

1. Introduction

Glucose directly participates in the metabolism of the human body and is the primary energy source for the human body. However, a high glucose level will damage the health of patients with diabetes. Several methods have been developed to detect glucose, including chromatography,[1] colorimetry,[2] fluorescence,[3] and electrochemical techniques.[4] Among them, electrochemical techniques show advantages of easy access to instruments, simple operation, and easy miniaturization. Electrochemical technology includes various methods, such as cyclic voltammetry (CV),[5] differential pulse voltammetry (DPV),[6] electrochemical impedance spectroscopy (EIS),[7] and chronoamperometry (CA), which can be flexibly applied. Enzyme electrochemical glucose sensors have high selectivity, but their sensitivity to environmental factors such as temperature, humidity, and pH affect their accuracy.[8] Therefore, enzyme-free electrochemical glucose sensors have received widespread attention. Various non-enzymatic materials, mainly nanomaterials, have been used for glucose sensors, which are known as nanoenzymes. For example, noble metals,[9,10] carbon-based nanomaterials,[11,12] and transition metal nanomaterials (mainly copper, cobalt, nickel, including their metals,[13,14] oxides,[15,16] hydroxides,[17,18] sulfides[19–23]) have been reported as electrode materials for electrochemical glucose sensing.

Transition metal sulfides have applications in the fields of photocatalysis,[24] supercapacitors,[25] sensors[26] and solar cells[27] due to their excellent physical and chemical properties, such as redox reversibility, capacitance and conductivity. Metal sulfides like CuS,[28] CoS[29] and NiS[30] were used as nanozymes for non-enzymatic glucose sensors. Li *et al.* prepared amorphous CoS on a reduced graphene oxide-poly(3,4-ethylenedioxythiophene) composite by electrodeposition, and the glucose sensor exhibited a linear range of 0.0002–1.38 mM, and sensitivity of 113.46 μA mM^{-1} cm^{-2} with a detection limit of 0.079 μM.[29] Lin *et al.* electrodeposited an α-NiS nanosphere film on ITO for glucose detection, and the sensor showed a linear range of 1–35 μM and a sensitivity of 8.4 μA μM^{-1} cm^{-2}.[30]

However, monometallic materials have few active sites and limited electrochemical activity, which limit their application in non-enzymatic glucose sensors. Enhanced electrochemical performance can be observed on electrodes based on multimetallic material due to their synergistic effect.[31,32] Binary metal sulfides have large redox reaction sites and high electrical conductivity compared to monometallic sulfides.[33] Vilian *et al.* prepared Ni_2CoS_4 nanopetals on carbon nanofibers (Ni_2CoS_4–CNF) by an electrospinning-assisted hydrothermal method. The Ni_2CoS_4–CNF-based glucose sensor exhibited an extremely low detection limit (0.25 nM) and a wide linear range (5–70 nM).[34] Cao *et al.* electrodeposited a nickel cobalt sulfide nanosheet film on a titanium mesh (Ni–Co–S/TM), which showed a wide linear response range of 0.001–3.0 mM, a sensitivity of 3291.5 μA mM^{-1} cm^{-2} and a low limit of detection of 0.12 μM for glucose sensing.[35]

Hubei University of Science and Technology, Xianning, Hubei, China. E-mail: stzjj@sina.com

† These authors contributed equally.

In addition to the type of electrode material, the electrode preparation method and morphology of the material have significant impacts on the performance of sensors. Generally, *in situ* preparation of materials on the electrode shows better sensing performance compared to an *ex situ* method due to good contact and direct electron transfer. For instance, Li *et al.* reported that electrodeposited CoS had better electrocatalytic activity than drop casting CoS for glucose sensing.[36] The *in situ* methods include electrospinning, electrodeposition, atomic vapor deposition, and the successive ionic layer adsorption and reaction (SILAR) method. The SILAR method has the advantages of low cost, fast speed, and easy operation. For instance, CuS,[37] CuO,[38] and Au nanoparticles[39] have been prepared on different substrates by SILAR to be used as glucose sensor electrodes. As for the morphology of the materials, nanomaterials with a small particle size and a larger specific surface area generally have more catalytic sites, better contact with electrolyte solution, and better electrocatalytic activity. These nanomaterials are usually pre-synthesized by a hydrothermal method and are later coated on the substrate by an *ex situ* method to prepare sensor electrodes. However, sensors prepared by an *ex situ* method generally have low sensitivity due to the poor contact between the material and the substrate.

In this work, monolayer cobalt nickel sulfide nanoparticles were prepared by SILAR on copper foam for non-enzymatic glucose detection. Copper foam has a larger surface area and better adsorption than ordinary smooth substrates (such as conductive glass and glassy carbon electrodes), so it is easier to use a SILAR method to prepare materials *in situ*. This method avoids the use of non-conductive connectors, allowing good contact between the material and substrate. Metal sulfide nanoparticles with a size smaller than 50 nm were grown on copper foam, which increased the catalytic performance of the electrode. Compared with single cobalt sulfide or nickel sulfide, the synergistic effect of bimetallic cobalt nickel sulfide significantly improved the performance of the sensor. The sensor exhibited high sensitivity and good repeatability and stability and was used to detect glucose in an actual sample. Most importantly, compared to other *in situ* methods, this method was simple and fast.

2. Experimental section

2.1. Materials

Glucose (Glu), NaOH, $Na_2S{\cdot}9H_2O$, $CoSO_4{\cdot}7H_2O$, and $NiSO_4{\cdot}6H_2O$ came from Kelong Reagent Co. Ltd (Chengdu, China). Uric acid (UA), dopamine, ascorbic acid (AA), and cysteine were bought from Wokai Biotechnology Co. Ltd (Shanghai, China). Methanol was bought from Sinopharm Chemical Reagent Co. Ltd. All of the above reagents were of analytical grade and used directly without further treatment. The serum sample was purchased from Shanghai Acmec Biochemical Co. Ltd.

2.2. Fabrication of CoNiS/CF

The optimized preparation process of the CoNiS/CF electrode was as follows: copper foam with an area of 1.5 × 0.8 cm^2 was ultrasonically cleaned with acetone, RO water and absolute ethanol in sequence for 10 min. As CoNiS has a large current response, to obtain electrodes with a low detection limit, the concentration of the precursor solution needs to be low, and the dipping time in the precursor solution need to be short. The naturally dried copper foam was immersed in a mixed solution of 0.05 M $CoSO_4$–$NiSO_4$ (Co/Ni molar ratio 3 : 1) for 10 s, which was then washed with deionized water to remove the residual solution and immersed in a solution of 0.05 M Na_2S for another 10 s. After that, it was washed with deionized water and dried at 50 °C for 3 h to obtain the CoNiS/CF electrode. A schematic diagram of electrode preparation using SILAR is shown in Fig. 1. To enhance the hydrophilicity of the copper foam, the solvent for both solutions was a mixed solvent of water and methanol ($V_{water}/V_{methanol}$ = 4 : 1). For comparison, CoS/CF and NiS/CF electrodes were prepared by the same procedure, except that the mixed solution was replaced with 0.05 M $NiSO_4$ or 0.05 M $CoSO_4$ solution.

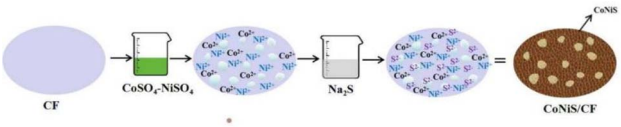

Fig. 1 Schematic of the fabrication of a CoNiS/CF electrode by the SILAR method.

2.3. Characteristics and electrochemical measurement

Scanning electron microscope (SEM) images were obtained from a Hitachi model SU 8020 UHR field emission scanning electron microscope (FESEM) (Japan), and the compositional analysis was performed by energy-dispersive X-ray spectroscopy (EDS). X-ray photo electron spectroscopy (XPS) analysis was tested with a Themo Escalab 250 (Thermo Fisher Scientific, USA) XPS system with a monochromatized Al Kα line source (1486.7 eV).

Cyclic voltammetry (CV) and chronoamperometry (CA) were performed with a three-electrode system on a CHI 760E electrochemical workstation (Chenhua Inc., China). The working electrode was the as-prepared electrode with an active area of 0.8 cm^2; the counter electrode was a Pt wire; and the reference electrode was an Ag/AgCl electrode. NaOH (0.1 M) was used as the electrolyte. CVs were performed in the potential window of 0–0.8 V at a scan rate of 20 mV s^{-1}.

3. Results and discussion

3.1. Characterization of CoNiS/CF

Fig. 2 shows the TEM and SEM images and EDS results of the CoNiS/CF electrode. Fig. 2(a and b) are the TEM images of CoNiS, which show that CoNiS nanoparticles were interconnected, and the size was less than 50 nm. As can be seen from Fig. 2(c), the copper foam surface was covered with a monolayer of rough aggregates. There were some relatively smooth areas which were irregular or nearly circular. These smooth areas were not connected but were independently and

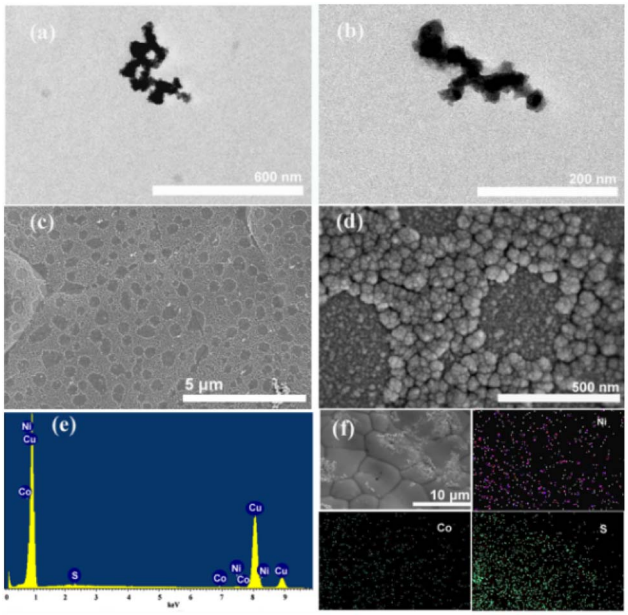

Fig. 2 TEM and SEM images and EDS of the CoNiS/CF electrode at (a) 600 nm scale, (b) 200 nm scale, (c) 5 μm scale, (d) 500 nm scale. (e) EDS spectrum, and (f) EDS mapping images of Ni, Co, S in scanned area.

uniformly distributed on the copper foam. Fig. 2(d) shows clearly that the rough area was a layer of aggregates that showed a cauliflower-like morphology, which is a typical structure of a sulfide. These aggregates had sizes of about 50–100 nm and were composed of smaller nanoparticles. During the SILAR process, the copper foam first adsorbed Co^{2+}–Ni^{2+} ions on its surface, and then S^{2-} ions were adsorbed; when S^{2-} ions met Co^{2+}–Ni^{2+} ions, they reacted immediately to form the CoNiS nanoparticles on the surface of the copper foam, forming the rough cauliflower-like morphology, which increased the specific surface area and added active sites for the electrocatalysis of glucose. It can be inferred from Fig. 1 that the rough area was the place where Co^{2+}–Ni^{2+} ions were adsorbed. In the Co^{2+}–Ni^{2+} ion adsorption process, the liquid film containing Co^{2+}–Ni^{2+} ions did not densely spread over the foam copper, but covered most of it, leaving some irregular or near circular smooth areas, which were the surface of foamed copper. Fig. 2(e) displays the EDS spectrum, indicating that Co, Ni, and S elements existed on the electrode. The map images in Fig. 2(f) demonstrate that Co, Ni, and S elements were distributed uniformly on the copper foam. The atomic ratio of Co to Ni was estimated to be 1 : 3.

The elemental composition of the CoNiS/CF electrode was analyzed by XPS. Fig. 3(a) is a full XPS spectrum, showing the presence of Co, Ni, and S elements in the material, where the presence of C and O is usually attributed to contamination caused by the use of carbon as a corrective material and oxygen adsorbed onto the material in the testing process, respectively. As Fig. 3(b) shows, peaks at binding energies of 856.5 eV and 874.1 eV correspond to $Ni2p_{3/2}$ and $Ni2p_{1/2}$ of Ni^{3+} with minor Ni^{2+}, respectively, and peaks at 862.1 eV and 880.1 eV are satellite peaks.[40,41] In Fig. 3(c), peaks at binding energies of 781.8 eV and 797.2 eV are ascribed to $Co2p_{3/2}$ and $Co2p_{1/2}$ of Co^{2+} with minor Co^{3+}, respectively, and satellite peaks are located at 786.7 eV and 803.2 eV.[40,41] Fig. 3(d) shows two peak at 162.4 eV and 163.2 eV, which are attributed to S 2p.[42] The above

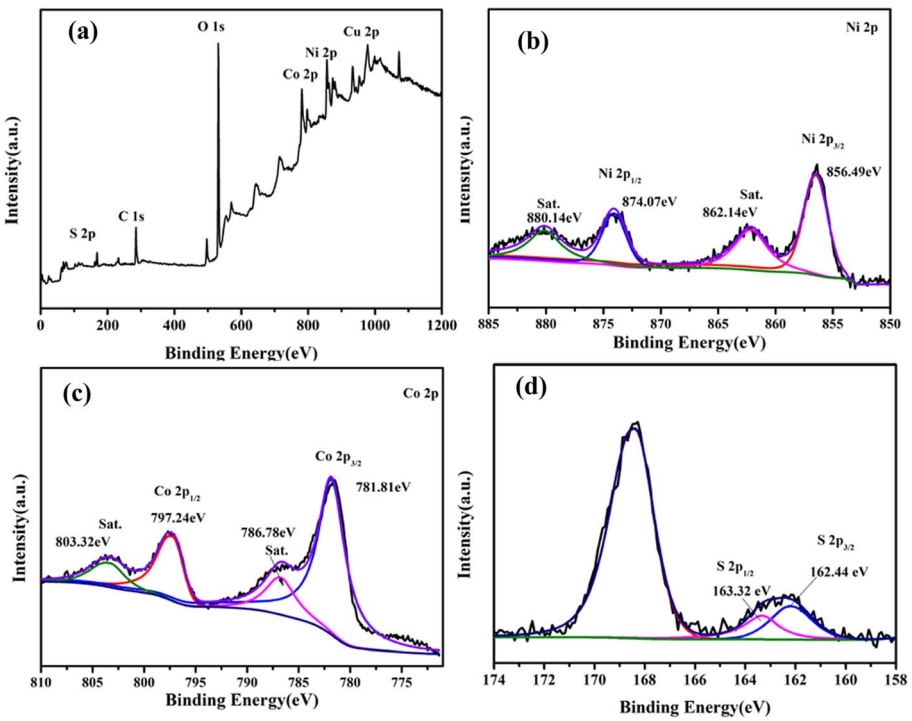

Fig. 3 XPS spectra of the CoNiS/CF electrode: (a) survey spectrum, (b) Ni 2p, (c) Co 2p and (d) S 2p.

results indicate that the CoNiS nanoparticles had been successfully grown on CF.

3.2. Electrochemical properties of CoNiS/CF

To study the electrochemical properties of the sensors, they were investigated by CV and CA. The CV curves of various electrodes with and without 0.5 mM glucose are presented in Fig. 4(a), which shows that the electrodes had oxidation peaks towards glucose at about 0.4–0.6 V. The oxidation peak currents increased significantly compared with those without glucose, indicating they all had an electrocatalytic effect on glucose. The bare CF had the lowest current responses, while the CoNiS/CF electrode exhibited current responses higher than those of CF or NiS/CF and close to those of CoS/CF. However, the current change before and after glucose addition for the CoNiS/CF electrode was larger than that of CoS/CF, indicating its better electrocatalytic activity for glucose. The feeding ratio of Co/Ni was optimized to achieve a better synergistic effect. From Fig. 4(b), a low oxidation peak current was obtained with a Co/Ni feeding ratio of 1 : 3; when the ratios were 3 : 1 and 5 : 1, the oxidation peak currents became higher, both nearing that of CoS/CF. Thus, the Co/Ni feeding ratio of 3 : 1 was ultimately used for the CoNiS/CF electrode. To improve the sensitivity of the CoNiS/CF electrode for glucose detection, its amperometric response was tested by adding 0.5 mM glucose to 0.1 M NaOH at different potentials (0.4, 0.5, 0.6, and 0.65 V). Fig. 4(c) shows that the current responses increased with the increase in potential; when the potential was greater than 0.6 V, the current responses no longer increased. Thus, 0.6 V was selected as the final detection potential. The CV curves of CoNiS/CF with different concentrations of glucose are shown in Fig. 4(d); the oxidation/reduction peak near 0.6 V increased gradually and linearly with an increase in glucose from 0.0 to 3.0 mM, indicating that the electrode was sensitive to glucose in this range.

Under alkaline conditions, Co^{2+} and Ni^{2+} change into Co^{3+} and Ni^{3+} at around 0.4–0.6 V; then Co^{3+} and Ni^{3+} react with glucose by electro-oxidation near 0.6 V to generate glucolactone. Therefore, in summary, the mechanism of electrocatalytic reactions between CoNiS/CF and glucose may include following processes:

$$CoS + OH^- \rightarrow CoSOH + e^- \quad (1)$$

$$NiS + OH^- \rightarrow NiSOH + e^- \quad (2)$$

$$Co^{3+} + \text{glucose} \rightarrow Co^{2+} + \text{gluconolactone} \quad (3)$$

$$Ni^{3+} + \text{glucose} \rightarrow Ni^{2+} + \text{gluconolactone} \quad (4)$$

The CV curves of the CoNiS/CF electrode towards glucose (0.3 mM in 0.1 M NaOH) with different scan rates are shown in Fig. 5(a). When scan rate went from 20 to 120 mV s^{-1}, the peak current intensity increased with the increase in scan rate. As shown in Fig. 5(b), the peak current of the redox peak of glucose was proportional to the square root of the scan rate, indicating that the redox reaction of glucose on this electrode was controlled by a diffusion process.

The current responses of the NiS/CF, CoS/CF, and CoNiS/CF electrodes were tested by CA with the addition of different concentrations of glucose to 0.1 M NaOH solution at a voltage of 0.6 V. The amperometric responses of the electrodes are shown

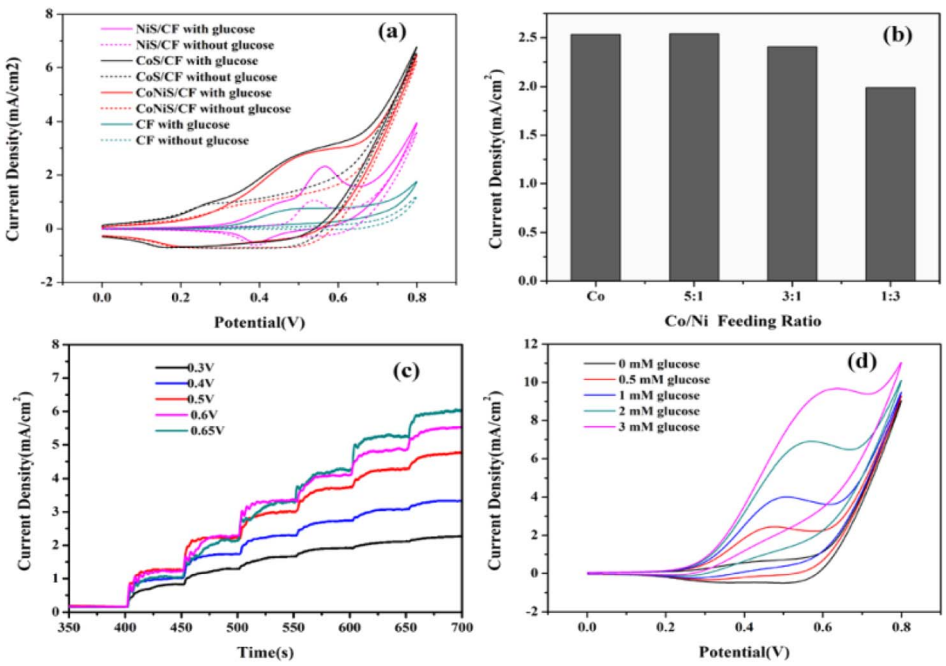

Fig. 4 (a) CVs of bare CF, NiS/CF, CoS/CF, and CoNiS/CF with and without 0.5 mM glucose in 0.1 M NaOH at a scan rate of 20 mV s^{-1}. (b) Oxidation peak currents of CoS/CF and CoNiS/CF with different Co/Ni feeding ratios. (c) Amperometric responses of the CoNiS/CF electrode with successive injections of 0.5 mM glucose at different potentials. (d) CVs of CoNiS/CF with different concentrations of glucose in 0.1 M NaOH at a scan rate of 20 mV s^{-1}.

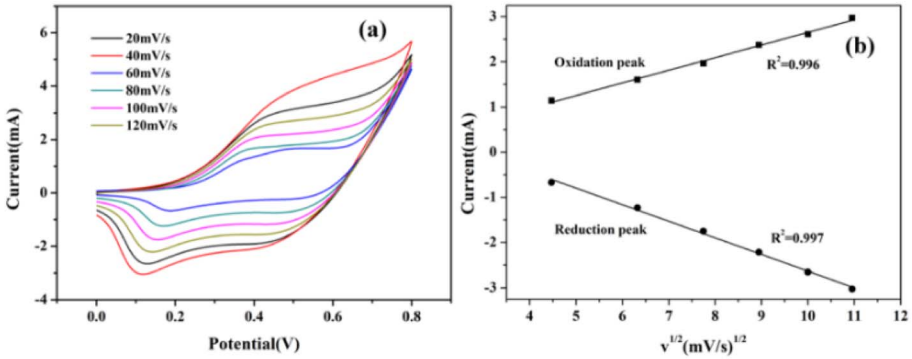

Fig. 5 (a) CVs of the CoNiS/CF electrode in 0.1 M KOH containing 0.3 mM glucose at different scan rates (20–120 mV s^{-1}). (b) Linear relationship between the oxidation/reduction peak current and square root of scan rate.

in Fig. 6(a), and their linear calibration plots are shown in Fig. 6(b–d). As shown in Fig. 6(b), the linear equation of NiS/CF was j (mA cm^{-2}) = 2.2365 C (mM) + 0.0029 with R^2 of 0.998, which showed a linear relationship with the glucose concentration in the range of 0.005–2.47 mM with a sensitivity of 2.2365 mA mM^{-1} cm^{-2} and a detection limit of 2.1 μM. Fig. 6(c) shows that Co/CF had a linear relationship in the range of 0.005–2.97 mM (j (mA cm^{-2}) = 1.8795 C (mM) + 0.0076, R^2 = 0.997), a sensitivity of 1.8795 mA mM^{-1} cm^{-2}, and a detection limit of 4.9 μM. Fig. 6(d) shows that CoNiS/CF had a linear relationship in the range of 0.005–3.47 mM (j (mA cm^{-2}) = 2.2987 C (mM) + 0.0038, R^2 = 0.995), a sensitivity of 2.2987 mA mM^{-1} cm^{-2}, and a detection limit of 2.0 μM. It can be seen that the electrochemical catalytic performance of CoNiS/CF was better than those of NiS/CF and CoS/CF, consistent with the results of CV measurement. Table 1 is a comparison of the performance of the as-prepared CoNiS/CF sensor with reported Co or Ni sulfide based glucose sensors. It can be seen from the table that our sensor had higher sensitivity and wider linearity than most of the listed sensors, indicating that the CoNiS/CF sensor prepared by this simple SILAR method showed good performance and might be used for the non-enzymatic detection of glucose.

3.3. Selectivity, reproducibility and stability

In actual glucose testing, common interfering substances in serum include ascorbic acid (AA), dopamine (DA), uric acid

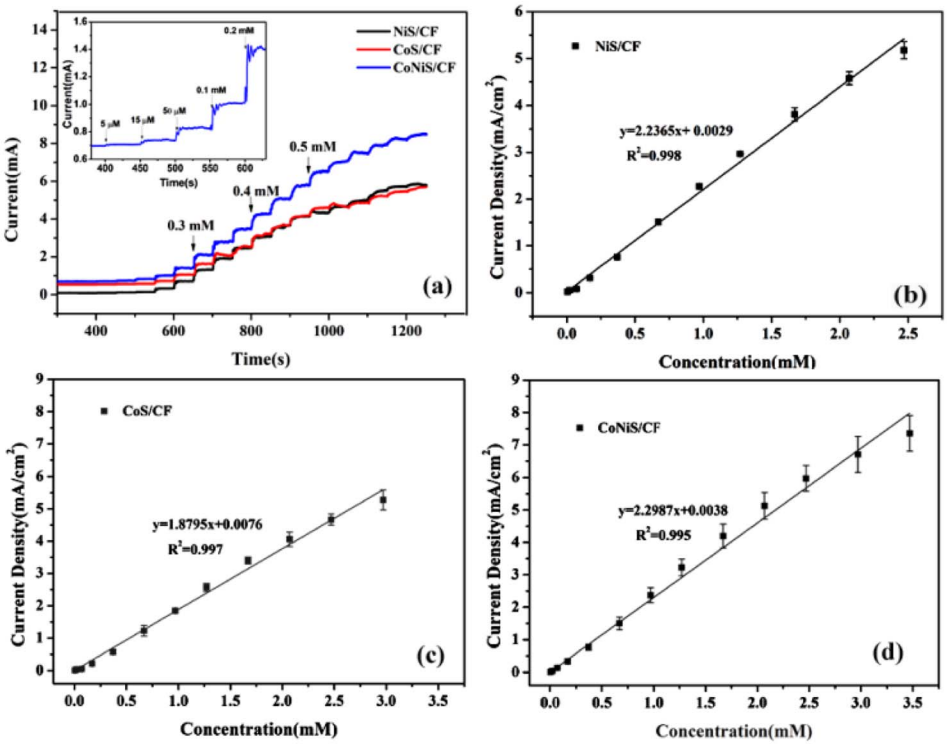

Fig. 6 Amperometric response of CoS/CF, NiS/CF and CoNiS/CF electrodes to glucose in 0.1 M NaOH under 0.6 V (a), and the corresponding linear relationship between the glucose concentration and current response of CoNiS/CF (b), CoS/CF (c), NiS/CF (d).

Table 1 Comparison of the sensing performance of the prepared CoNiS/CF sensor with previously reported sensors

Electrode	Sensitivity (μA mM^{-1} cm^{-2})	Linear range (mM)	Detection limit (μM)	Ref.
NiCoS/Ti mesh	3290	0.001–3.0	0.12	34
CoS-ED	330	0.08–1.0	—	36
CoS@C/GCE	697	0.01–0.96	2.0	43
CoS-PPy-CP	1110	0.0005–0.4665	0.14	44
CoS/Co-MOF	4600	0.005–1.17	0.11	45
NiS	5.78	0.005–0.06	0.052	46
NiS	54.6	0.02–5.0	0.0083	47
NiS/S-g-C_3N_4	80	0.001–2.1	1.5	48
$NiCo_2S_4$/EGF-7	7431.96	0.0005–3.571	0.167	49
P-$NiCo_2S_4$/ITO	250	0.001–5.2	0.46	50
$NiCo_2S_4$/GCE	858.57	0.005–0.1	2.0	51
$NiCo_2S_4$/FTO	1890	0.2–2.4	2.226	52
$NiCo_2S_4$/Ni/CFP	283	0.0005–6.0	0.0005	53
CoNiS/CF	2298.7	0.005–3.47	2.0	This work

(UA), and cysteine, whose concentrations are approximately 10% of glucose concentration. Therefore, selective testing is essential. The procedure was as follows: 0.1 mM of glucose, 0.01 mM of AA, DA, UA, cysteine and 0.1 mM of glucose were added to 0.1 M NaOH solution; their amperometric responses are recorded in Fig. 7(a). No interferents produced an evident current response, whereas the additions of 0.1 M glucose before and after the interferents produced significant and almost identical current responses, respectively, indicating that the CoNiS/CF electrode showed good selectivity to glucose.

Reproducibility and stability are also important factors for evaluating sensors. Five independent CoNiS/CF electrodes were used to measure 0.6 M glucose under same conditions. The relative standard deviation (RSD) of the five amperometric current responses was 4.0% (Fig. 7(b)). The long-term stability of CoNiS/CF electrodes was tested by recording the first current response value I_0 toward 0.5 mM glucose in 0.1 M NaOH. They were then stored in a 2–4 °C refrigerator, and the current response intensity I was tested every five days under same conditions. As shown in Fig. 7(c), after 25 days, the current

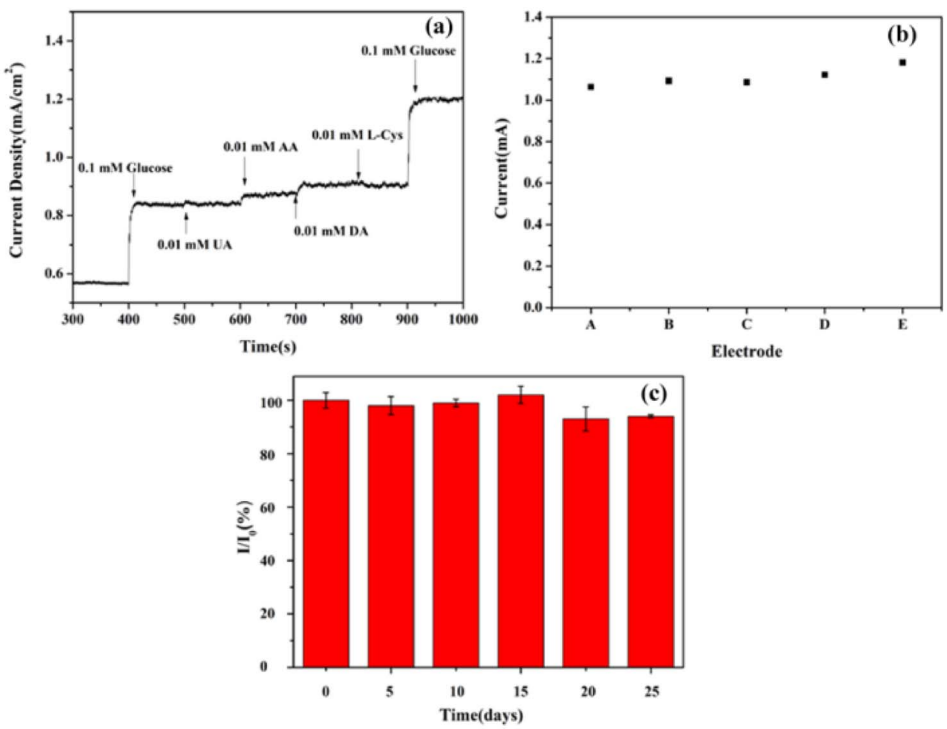

Fig. 7 (a) Amperometric curves of the CoNiS/CF electrode with the successive addition of 0.1 mM of glucose, 0.01 mM of UA, AA, DA and cysteine in 0.1 M NaOH. (b) Amperometric currents of five pieces of independent CoNiS/CF electrodes towards 0.5 mM glucose. (c) Stability of CoNiS/CF electrodes to 0.6 mM glucose tested every 5 days for 25 days.

Table 2 Comparison of standard glucose concentration and concentration measured with the CoNiS/CF sensor

Sample	Standard concentration (μM)	Measured concentration (μM)	Recovery (%)	RSD (%) $n = 5$
1	450	465	103.3	4.50
2	500	525	105.0	3.95
3	550	569	103.4	4.34

intensity ratio I/I_0 of the CoNiS/CF electrode remained above 93%, indicating that the electrodes showed good stability and could withstand long-term continuous glucose testing.

To examine the practicality of the CoNiS/CF electrode, commercial serum was added to 0.1 M NaOH containing standard glucose solution under constant stirring (the added serum was diluted 1000 times), the current response was recorded by CA, and the glucose content was calculated according to the linear equation. The recoveries of the three samples were 103.3–105.0%, and the RSD of all test results was less than 5.0% (Table 2), indicating that the sensor was feasible for the detection of actual samples.

4. Conclusions

In summary, a novel CoNiS/CF electrode was fabricated by the SILAR method for an enzyme-free glucose sensor. The optimized electrode enhanced the electrochemical response and increased the sensing performance through the synergistic effect of cobalt and nickel. The sensor was found to have good electrocatalytic activity for glucose oxidation in 0.1 M NaOH solution, which exhibited a linear range of 0.005–3.47 mM, a sensitivity of 2298.7 μA mM^{-1} cm^{-2}, and a detection limit of 2.0 μM. In addition, the sensor showed good selectivity, reproducibility and stability. It also achieved satisfactory recoveries in real serum sample measurement, indicating the application feasibility of a CoNiS/CF electrode. This study provides a simple and fast method for the *in situ* preparation of electrodes for high-sensitivity glucose sensors.

Author contributions

Shi Wang: conceptualization, formal analysis, writing – original draft. Ruirui Zhang: conceptualization, methodology. Ning Li: validation, visualization, formal analysis. Jialin Ao: validation, visualization. Saiwen Ding: investigation, formal analysis. Ting Shu: conceptualization, methodology, writing – review & editing, supervision.

Conflicts of interest

There are no conflicts to declare.

Acknowledgements

This work was supported by the Educational Commission of Hubei Province of China (D20222802).

Notes and references

1 Y. Zhou, J. P. Chen, L. Gan, W. Xu, Y. Liu, Y. G. Zhao and Y. Zhu, *J. Chromatogr.*, 2022, **1685**, 463564.
2 M. Srivastava, S. K. Srivastava, R. P. Ojha and R. Prakash, *Microchem. J.*, 2022, **182**, 107850.
3 S. K. Vaishanav, J. Korram, R. Nagwanshi, K. K. Ghosh and M. L. Satnami, *Sens. Actuators, B*, 2017, **245**, 196–204.
4 H. Kim, H. Choi, C. S. Park, H. S. Yim, D. Kim, S. Lee and Y. Lee, *Biosensors*, 2023, **13**, 248.
5 N. Sheibani, M. Kazemipour, S. Jahani and M. M. Foroughi, *Microchem. J.*, 2019, **149**, 103980.
6 T. Iranmanesh, S. Jahani, M. M. Foroughi, M. S. Zandi and H. H. Nadiki, *Anal. Methods*, 2020, **12**, 4319–4326.
7 M. M. Foroughi, S. Jahani, S. Rashidi, O. Tayari and M. Moradalizadeh, *Mater. Chem. Phys.*, 2024, **315**, 128893.
8 N. Lu, C. L. Shao, X. H. Li, F. J. Miao, K. X. Wang and Y. C. Liu, *Ceram. Int.*, 2016, **42**, 11285–11293.
9 K. Shim, W. C. Lee, M. S. Park, M. Shahabuddin, Y. Yamauchi, M. S. A. Hossain, Y. B. Shim and J. H. Kim, *Sens. Actuators, B*, 2019, **278**, 88–96.
10 F. Li, X. Chen, H. Wang, M. Liu and H. L. Peng, *ACS Appl. Mater. Interfaces*, 2023, **15**, 13290–13298.
11 C. Tiwari, S. S. Jha, R. Kumar, M. Chhabra, B. D. Malhotra and A. Dixit, *Mater. Sci. Eng., B*, 2022, **285**, 115931.
12 J. Mohapatra, B. Ananthoju, V. Nair, A. Mitra, D. Bahadur, N. V. Medhekar and M. Aslam, *Appl. Surf. Sci.*, 2018, **442**, 332–341.
13 M. Pak, A. Moshaii, H. Siampour, S. Abbasian and M. Nikkhah, *Microchim. Acta*, 2020, **187**, 276.
14 G. Mo, X. Zheng, N. Ye and Z. Ruan, *Talanta*, 2021, **225**, 121954.
15 S. Sedaghat, C. R. Piepenburg, A. Zareei, Z. Qi, S. Peana, H. Wang and R. Rahimi, *ACS Appl. Nano Mater.*, 2020, **3**, 5260–5270.
16 W. Liu, G. Chai, X. Zhao, Y. Dai and Y. Qi, *Sens. Actuators, B*, 2020, **321**, 128485.
17 N. Shi, S. Sun, B. Zhang, Q. Du, Y. Liao, X. Liao, G. Yin, Z. Huang, X. Pu and X. Chen, *Nanotechnology*, 2020, **31**, 325502.
18 J. Tashkhourian, S. F. Nami-Ana and M. Shamsipur, *Anal. Chim. Acta*, 2018, **1034**, 63–73.
19 B. Kim, S. H. Lee, M. Cho and Y. Lee, *Sens. Actuators, B*, 2017, **249**, 161–167.
20 M. Keerthi, B. Mutharani, S. M. Chen and P. Ranganathan, *Microchim. Acta*, 2019, **186**, 807.
21 J. Zhua, X. Penga, W. Nie, Y. Wang, J. Gao, W. Wen, J. N. Selvaraj, X. Zhang and S. Wang, *Biosens. Bioelectron.*, 2019, **141**, 111450.
22 W. Wu, B. Yu, H. Wu, S. Wang, Q. Xia and Y. Ding, *Mater. Sci. Eng., C*, 2017, **70**, 430–437.
23 P. K. Kannan and C. S. Rout, *Chem.–Eur. J.*, 2015, **21**, 9355–9359.
24 S. Khan, H. Choi, D. Kim, S. Y. Lee, Q. Zhu, J. Zhang, S. Kim and S. H. Cho, *Chem. Eng. J.*, 2020, **395**, 125092.

25 R. Barik and P. P. Ingole, *Curr. Opin. Electrochem.*, 2020, **21**, 327–334.
26 B. Chatterjee and A. Bandyopadhyay, *Mater. Sci. Eng., B*, 2023, **297**, 116781.
27 L. H. Kharboot, N. A. Fadil, T. A. A. Bakar, A. S. M. Najib, N. H. Nordin and H. Ghazali, *Materials*, 2023, **16**, 2881.
28 K. P. Sharma, M. Shin, G. P. Awasthi, M. B. Poudel, H. J. Kim and C. Yu, *Int. J. Biol. Macromol.*, 2022, **206**, 708–717.
29 A. Meng, L. Sheng, K. Zhao and Z. Li, *J. Mater. Chem. B*, 2017, **5**, 8934–8943.
30 S. Lin, J. B. Shi, C. M. Peng, B. C. Zheng, F. C. Cheng, M. W. Lee, H. W. Lee, P. F. Wu and Y. J. Liu, *Nanoscale Res. Lett.*, 2018, **13**, 109.
31 W. Li, S. Lv, Y. Wang, L. Zhang and X. Cui, *Sens. Actuators, B*, 2019, **281**, 652–658.
32 J. Ding, L. Zhong, X. Wang, L. Chai, Y. Wang, M. Jiang, T. T. Li, Y. Hua, J. Qian and S. Huang, *Sens. Actuators, B*, 2020, **306**, 127551.
33 P. Kulkarni, S. K. Nataraj, R. G. Balakrishna, D. H. Nagaraju and M. V. Reddy, *J. Mater. Chem. A*, 2017, **5**, 22040–22094.
34 E. Vilian, S. K. Hwang, K. S. Ranjith, Y. Cho, Y. S. Huh and Y. K. Han, *Microchim. Acta*, 2021, **188**, 106.
35 X. Cao, K. Wang, G. Du, A. M. Asiri, Y. Ma, Q. Lu and X. Sun, *J. Mater. Chem. B*, 2016, **4**, 7540–7544.
36 X. Li, S. Sharma, D. W. M. Arrigan and D. S. Silvester, *J. Electrochem. Soc.*, 2022, **169**, 056505.
37 C. Wei, X. Zou, Q. Liu, S. Li, C. Kang and W. Xiang, *Electrochim. Acta*, 2020, **334**, 135630.
38 A. S. Patil, R. T. Patil, G. M. Lohar and V. J. Fulari, *Appl. Phys. A*, 2021, **127**, 101.
39 J. Li, L. Yan, H. Wang, H. Wang, X. Chen, L. Wang and M. Wu, *J. Mater. Sci.: Mater. Electron.*, 2017, **8**, 3067–3074.
40 J. Yang, M. Cho and Y. Lee, *Biosens. Bioelectron.*, 2016, **75**, 15–22.
41 W. Li, S. Lv, Y. Wang, L. Zhang and X. Cui, *Sens. Actuators, B*, 2019, **281**, 652–658.
42 X. Liu, L. Ai and J. Jiang, *Powder Technol.*, 2015, **283**, 539–548.
43 P. Qu, Z. Gong, H. Cheng, W. Xiong, X. Wu, P. Pei, R. Zhao, Y. Zeng and Z. Zhu, *RSC Adv.*, 2015, **5**, 106661–106667.
44 Y. Qi, Y. Hu, X. Wu, W. Wu, J. Bao, H. Yang, J. Zhao, C. Hou and D. Huo, *J. Electrochem. Soc.*, 2021, **168**, 107507.
45 S. Ramesh, A. T. A. Ahmed, Y. Haldorai, V. Kakani, C. Bathula and H. S. Kim, *J. Alloys Compd.*, 2023, **967**, 171760.
46 R. Singh and M. M. Ayyub, *ACS Appl. Electron. Mater.*, 2021, **3**, 1912–1919.
47 M. Arivazhagan, Y. M. Santhosh and G. Maduraiveeran, *Micromachines*, 2021, **12**, 403.
48 S. Vinot, P. M. Rajaitha, A. Venkadesh, K. S. S. Devi, S. Radhakrishnan and A. Pandikumar, *Nanoscale Adv.*, 2020, **2**, 4242–4250.
49 Q. Guo, T. Wu, L. Liu, Y. He, D. Liu and T. You, *J. Alloys Compd.*, 2020, **819**, 153376.
50 X. Lang, D. Chu, Y. Wang, D. Ge and X. Chen, *Biosensors*, 2022, **12**, 823.
51 D. Chen, H. Wang and M. Yang, *Anal. Methods*, 2017, **9**, 4718–4725.
52 H. Yuan, C. Ma, Z. Gao and L. Zhang, *Appl. Phys. A*, 2019, **125**, 61.
53 K. J. Babu, T. R. Kumar, D. J. Yoo, S. M. Phang and G. Gnana Kumar, *ACS Sustainable Chem. Eng.*, 2018, **6**, 16982–16989.